

PAPER • OPEN ACCESS

Steady-state entanglement production in a quantum thermal machine with continuous feedback control

To cite this article: Giovanni Francesco Diotallevi *et al* 2024 *New J. Phys.* **26** 053005

View the [article online](#) for updates and enhancements.

You may also like

- [Pseudomode treatment of strong-coupling quantum thermodynamics](#)
Francesco Albarelli, Bassano Vacchini and Andrea Smirne
- [Quasi-autonomous quantum thermal machines and quantum to classical energy flow](#)
Max F Frenzel, David Jennings and Terry Rudolph
- [Critical heat current for operating an entanglement engine](#)
Shishir Khandelwal, Nicolas Palazzo, Nicolas Brunner et al.



PAPER

Steady-state entanglement production in a quantum thermal machine with continuous feedback control

OPEN ACCESS

RECEIVED

29 November 2023

REVISED

26 February 2024

ACCEPTED FOR PUBLICATION






16 April 2024

PUBLISHED

7 May 2024

Original Content from
this work may be used
under the terms of the
[Creative Commons
Attribution 4.0 licence](#).

Any further distribution
of this work must
maintain attribution to
the author(s) and the title
of the work, journal
citation and DOI.

Giovanni Francesco Diotallevi^{1,2,*} , Björn Annby-Andersson¹ , Peter Samuelsson¹ , Armin Tavakoli¹ 
and Pharnam Bakhshinezhad^{1,3,*} ¹ Physics Department and NanoLund, Lund University, Box 118, 22100 Lund, Sweden² Augsburg University, Institute of Physics, Universitätsstraße 1 (Physik Nord), Augsburg 86159, Germany³ Atominstytut, Technische Universität Wien, Stadionallee 2, 1020 Vienna, Austria

* Authors to whom any correspondence should be addressed.

E-mail: francesco.diotallevi@uni-a.de and pharnam.bakhshinezhad@tuwien.ac.at**Keywords:** steady state, feedback, entanglement generation, thermal machine, heat current**Abstract**

Quantum thermal machines can generate steady-state entanglement by harvesting spontaneous interactions with local environments. However, using minimal resources and control, the entanglement is typically weak. Here, we study entanglement generation in a two-qubit quantum thermal machine in the presence of a continuous feedback protocol. Each qubit is measured continuously and the outcomes are used for real-time feedback to control the local system-environment interactions. We show that there exists an ideal operation regime where the quality of entanglement is significantly improved, to the extent that it can violate standard Bell inequalities and uphold quantum teleportation. In agreement with (Khandelwal *et al* 2020 *New J. Phys.* **22** 073039), we also find, for ideal operation, that the heat current across the system is proportional to the entanglement concurrence. Finally, we investigate the robustness of entanglement production when the machine operates away from the ideal conditions.

1. Introduction

Quantum thermal machines are quantum systems coupled to two, or several, thermal reservoirs, which exploit temperature gradients to perform useful tasks such as cooling, heating, timekeeping, and producing work [1–3]. In contrast to their classical counterparts, these machines rely on quantum features, like entanglement and tunneling. Therefore, they are promising testbeds for studying fundamental aspects of quantum physics, such as the generation, stabilization, and control of entanglement in the presence of thermal environments.

To this end, it was shown that a minimal quantum thermal machine, consisting of two coherently interacting qubits coupled to two reservoirs at different temperatures, is able to produce stationary entangled states [4]. The word ‘minimal’ refers to the minimal setup required to generate entanglement. The success of this machine can be linked to the magnitude of the heat current flowing through the system [5]. However, the entanglement generated in such a machine is typically weak and noisy. For example, it is unable to perform well-known entanglement-based tasks such as teleportation or Bell inequality violation [6]. Therefore, in order to improve the entanglement production, it has been considered to supply the original autonomous system with some additional resources. It has been found that heralding the output state of a multi-dimensional autonomous quantum thermal machine, via a local measurement, can generate maximally entangled states [7]. This type of approach also enables multipartite entanglement production [8]. However, this requires coherent control of multi-level systems and the ability to perform non-demolition filter measurements. An alternative approach is to introduce a third bath that is common to both qubits [9], which leads to an improvement in the entanglement production. Another approach that improves the entanglement is to perform a population inversion process in fermionic baths [6]. This amounts to bath engineering, but can improve entanglement production to the extent that non-trivial teleportation fidelities

are possible. Complementary to that, by implementing the minimal machine in a double quantum dot, a large voltage bias can be applied across the system to generate entanglement that is nonlocal [10].

In this paper, we investigate how the entanglement of the quantum thermal machine of [3] can be controlled and improved using measurement-based feedback control. This route is independent of the experimental platform. We note that the idea of using measurement-based feedback to increase entanglement is not new, but has previously been explored in optical systems [11–16], where qubits enclosed in optical cavities are externally driven via feedback control. However, the lack of thermal environments and time-independent coherent interactions in the cited literature is a clear distinction from our setup. Our feedback protocol is based on a continuous parity measurement of the qubits, distinguishing whether one of the qubits are excited or if both are in the ground or excited state. If only one qubit is excited, the warmer bath is decoupled from the system, favoring coherent interactions between the qubits. If no or two excitations reside in the system, the hot bath is re-coupled to the qubits. The protocol is modeled by employing the quantum Fokker–Planck master equation presented in [17], which was developed to describe continuous, Markovian feedback protocols like the one presented here. To facilitate a direct comparison with previous relevant works, we use the concurrence to quantify the entanglement, as well as investigate operational aspects of the nonclassicality of the produced entanglement [6]. We identify an optimal operation regime where the concurrence significantly exceeds what was found in the elementary machine [4]. Additionally, we find that the entanglement can violate the CHSH inequality and uphold quantum teleportation. In particular, we find, in the optimal regime, that the concurrence is proportional to the heat current flowing between the reservoirs, implying that a nonzero heat current is an entanglement witness. This contrasts the elementary machine, in which the heat current must exceed a non-trivial threshold to act as an entanglement witness [5]. We note that the results obtained in the optimal operation regime are independent whether the thermal reservoirs are bosonic or fermionic. We also investigate the robustness of the entanglement production when relaxing the ideal conditions. We find that the entanglement decreases, while still being larger than in the absence of feedback.

The paper is structured as follows. In section 2, we briefly review the system and the concurrence as a measure for entanglement. Section 3 introduces the feedback protocol and how it is modeled. In section 4, we present our results, and section 5 concludes the paper.

2. System and entanglement

We consider two coherently interacting qubits coupled to two thermal reservoirs with temperatures T_C and T_H ($T_C < T_H$) as depicted in figure 1. Note that the coherent interaction is autonomous, and does not rely on external driving. The reservoirs can be fermionic or bosonic, but as many of the results are independent of particle type, we introduce the system without specifying particle type, keeping the discussion general. If particle type matters, we will clearly specify this. We consider the following Hamiltonian of the qubits,

$$\hat{H} = \varepsilon(|1\rangle\langle 1|_C \otimes \mathbb{1} + \mathbb{1} \otimes |1\rangle\langle 1|_H) + g(|01\rangle\langle 10| + |10\rangle\langle 01|) + U|11\rangle\langle 11|, \quad (1)$$

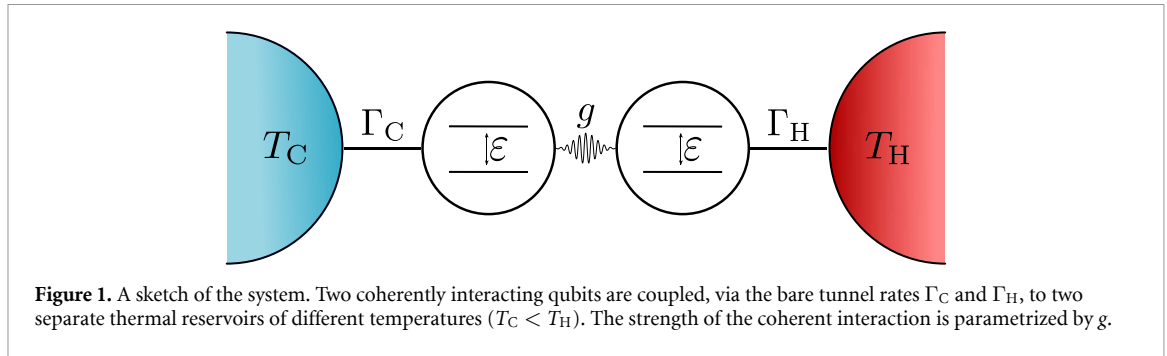
where $|0\rangle$ and $|1\rangle$ denote the ground and excited states of the qubits, $\mathbb{1}$ is the identity operator, ε is the energy of the excited state of each qubit, g is the strength of the coherent flip-flop interaction, and U is the interaction energy between the excited states. The last term naturally arises when the excitations carry charge. This Hamiltonian can be experimentally realized in double quantum dots [18, 19] and superconducting circuits [20]. In the double dot system, the interaction energy U corresponds to the Coulomb interaction between electrons, and is non-zero. Typically, it is easy to establish a scenario where $U \rightarrow \infty$ is a good approximation. For superconducting circuits, $U = 0$ (see the supplementary material of [20]).

By assuming weak system-bath and qubit-qubit interactions, the dynamics of the system can be written as a local Lindblad master equation (we set $\hbar = 1$),

$$\partial_t \hat{\rho} = \mathcal{L} \hat{\rho} = i[\hat{\rho}, \hat{H}] + \sum_{\substack{k \in \{C,H\} \\ l \in \{0,1\}}} \left(\Gamma_{kl}^+ \mathcal{D}[\hat{J}_{kl}^\dagger] + \Gamma_{kl}^- \mathcal{D}[\hat{J}_{kl}] \right) \hat{\rho}, \quad (2)$$

where we introduced the shorthand superoperator notation \mathcal{L} , describing the dynamics of the system. The dissipators $\mathcal{D}[\hat{J}_{kl}] \hat{\rho} \equiv \hat{J}_{kl} \hat{\rho} \hat{J}_{kl}^\dagger - \frac{1}{2} \left\{ \hat{J}_{kl}^\dagger \hat{J}_{kl}, \hat{\rho} \right\}$, where $\hat{J}_{C0} = |00\rangle\langle 10|$, $\hat{J}_{C1} = |01\rangle\langle 11|$, $\hat{J}_{H0} = |00\rangle\langle 01|$, and $\hat{J}_{H1} = |10\rangle\langle 11|$ are jump operators describing bath-induced de-excitations of the qubits with corresponding excitation (+) and de-excitation (−) rates

$$\Gamma_{kl}^+ = \frac{\Gamma_k}{e^{(\varepsilon+U)/T_k} \pm 1}, \quad \Gamma_{kl}^- = \frac{\Gamma_k}{1 \pm e^{-(\varepsilon+U)/T_k}}, \quad (3)$$



where Γ_k is the bare transition rate for bath k (see figure 1), and the + (−) in the denominators corresponds to fermionic (bosonic) reservoirs. Note that the chemical potentials of the baths are set to zero and we have set the Boltzmann constant $k_b = 1$. From here on, we normalize all energies with respect to ε , i.e. effectively setting $\varepsilon = 1$.

The stationary state of equation (2) takes the form

$$\hat{\varrho}_\infty = \begin{bmatrix} \varrho_{00} & 0 & 0 & 0 \\ 0 & \varrho_{01} & \alpha & 0 \\ 0 & \alpha^* & \varrho_{10} & 0 \\ 0 & 0 & 0 & \varrho_{11} \end{bmatrix}, \quad (4)$$

when written in the computational basis $\{|00\rangle, |01\rangle, |10\rangle, |11\rangle\}$. Note that $\sum_{i,j=0}^1 \varrho_{ij} = 1$ and $|\alpha| \leq \sqrt{\varrho_{01}\varrho_{10}}$ ensure the normalization and positivity of $\hat{\varrho}$. This form in equation (4) arises because of the flip-flop interaction in the Hamiltonian in equation (1) and the dissipative interactions between the system and the reservoirs, only allowing coherent interaction in the subspace $\{|01\rangle, |10\rangle\}$ such that the remaining coherences vanish for long times. To quantify the entanglement in the stationary state, we use the concurrence [21], which is an entanglement monotone for bipartite systems that can identify fully separable and maximally entangled states. For the state in equation (4), the concurrence takes the form [6]

$$\mathcal{C}(\hat{\varrho}_\infty) = \max\{2(|\alpha| - \sqrt{\varrho_{00}\varrho_{11}}), 0\}, \quad (5)$$

taking values between 0 and 1, where 0 corresponds to $\hat{\varrho}_\infty$ being fully separable and 1 to being maximally entangled. Values different from 0 and 1 correspond to states containing partial amounts of entanglement. In [4] it was shown that the maximal stationary concurrence is given by $\mathcal{C} \sim 0.09$ (0.25) for bosonic (fermionic) particles. The difference in performance is due to $U \neq 0$ for fermions, which is naturally the case for, e.g. electrons. However, the entanglement generated this way is not useful in several operational notions of nonclassicality, such as steering, nonlocality and teleportation [6].

3. Feedback protocol

To increase the entanglement, it is necessary to transfer population from the $\{|00\rangle, |11\rangle\}$ subspace to the $\{|01\rangle, |10\rangle\}$ subspace, while simultaneously maximizing the coherence α in the latter subspace, see equations (4) and (5). To this end, we introduce a feedback protocol, controlling the coupling between the system and the hot reservoir. The control procedure follows an on-off protocol [22] and is conditioned on measuring the parity of the qubits, see the qualitative sketch in figure 2. Note that when measuring parity, it is not possible to distinguish which of the qubits that is excited. Therefore, the measurement does not affect the coherence α . When a single excitation resides in the system, the hot bath is decoupled from the hot qubit. An excitation in the hot qubit can thus only interact with the cold qubit, and not dissipate into the hot bath. This reduces ϱ_{00} and ϱ_{11} , while increasing the coherently coupled populations ϱ_{01} and ϱ_{10} . Also note that the decoherence induced by the hot bath is suppressed, shielding the coherence of the system. With no, or two, excitations in the system, the hot bath is re-coupled, again allowing thermal excitation of the hot qubit. Note that it is not useful to additionally close the coupling to the cold reservoir, as excitations would oscillate between the qubits indefinitely, preventing stationary entanglement production.

Mathematically, we formulate the feedback protocol in the following way. We continuously measure the parity observable

$$\hat{A} = \hat{\sigma}_z \otimes \hat{\sigma}_z, \quad (6)$$

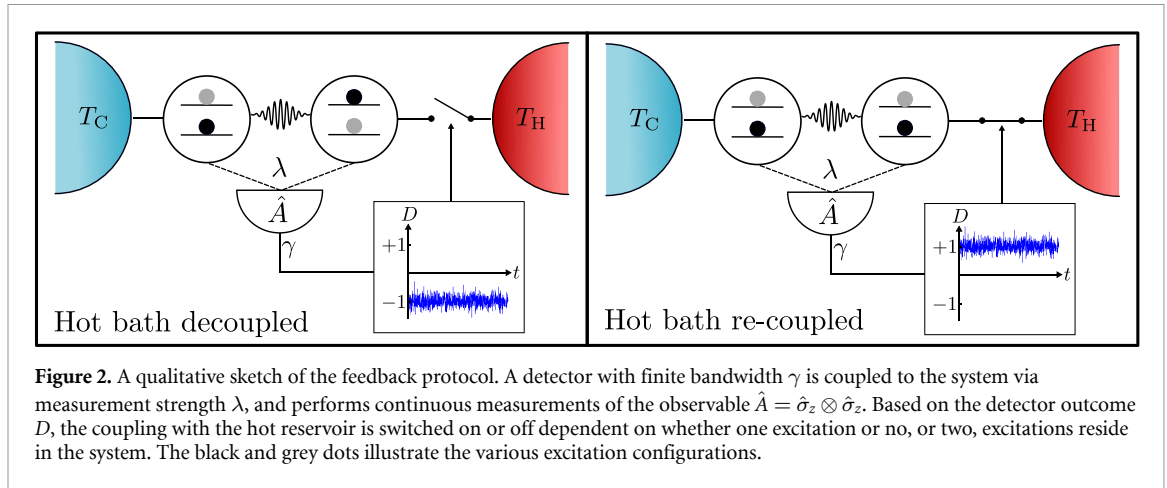


Figure 2. A qualitative sketch of the feedback protocol. A detector with finite bandwidth γ is coupled to the system via measurement strength λ , and performs continuous measurements of the observable $\hat{A} = \hat{\sigma}_z \otimes \hat{\sigma}_z$. Based on the detector outcome D , the coupling with the hot reservoir is switched on or off dependent on whether one excitation or no, or two, excitations reside in the system. The black and grey dots illustrate the various excitation configurations.

where $\hat{\sigma}_z$ is the Pauli-Z matrix. Note that $[\hat{A}, \hat{\rho}_\infty] = 0$ for the density matrix in equation (4). This results in a backaction-free measurement, which is a class of measurements sometimes also known as quantum nondemolition measurements [17, 23, 24]. This means that the coherence in equation (4) will not be affected by the measurement. As a result, the measurement is not detrimental for the entanglement production. The detector output D is noisy, with fluctuations around -1 when the system occupies $|01\rangle$ or $|10\rangle$, and around $+1$ when occupying $|00\rangle$ or $|11\rangle$, see the time traces in figure 2. We thus interpret the signal as follows. When $D < 0$, we assume that $|01\rangle$ or $|10\rangle$ is occupied. For $D > 0$, we assume that $|00\rangle$ or $|11\rangle$ is occupied.

To describe the dynamics of the system under the feedback protocol, we make use of the quantum Fokker-Planck master equation introduced in [17]. This formalism allows us to describe the dynamics of any quantum system undergoing continuous, Markovian feedback control. For our protocol, it reads

$$\partial_t \hat{\rho}_t(D) = \mathcal{L}(D) \hat{\rho}_t(D) - \gamma \partial_D \mathcal{A}(D) \hat{\rho}_t(D) + \frac{\gamma^2}{8\lambda} \partial_D^2 \hat{\rho}_t(D),$$

where $\hat{\rho}_t(D)$ is the joint system-detector state, with $\hat{\rho}_t = \int dD \hat{\rho}_t(D)$ being the system state independent of the detector, and $p_t(D) = \text{tr}\{\hat{\rho}_t(D)\}$ being the probability distribution of observing outcome D at time t . Note that $\int dD \text{tr}\{\hat{\rho}_t(D)\} = 1$.

The feedback-controlled dynamics of the system are described by

$$\mathcal{L}(D) = \theta(D) \mathcal{L} + [1 - \theta(D)] \tilde{\mathcal{L}}, \tag{7}$$

where \mathcal{L} is given by equation (2) and describes the dynamics when the hot bath is coupled to the system, while $\tilde{\mathcal{L}} \hat{\rho} = i[\hat{\rho}, \hat{H}] + \sum_{l \in \{0,1\}} (\Gamma_{Cl}^+ \mathcal{D}[\hat{J}_{Cl}^\dagger] + \Gamma_{Cl}^- \mathcal{D}[\hat{J}_{Cl}]) \hat{\rho}$ describes the dynamics when decoupling the hot bath.

The remaining two terms of equation (7) constitute a Fokker-Planck equation describing the time evolution of the detector. In short, the detector's dynamics are treated as those of a random walker relaxing towards a value dictated by the state of the system. The superoperator drift coefficient $\mathcal{A}(D) \hat{\rho} \equiv \frac{1}{2} \{\hat{A} - D, \hat{\rho}\}$ describes the coupling between the system and detector, and determines the average position of the detector, dependent on the system state. Note that γ is the bandwidth of the detector, such that $1/\gamma$ gives the lag of the detector. The last term describes the diffusion of the detector position, where the diffusion constant $\gamma/8\lambda$ corresponds to the noise of the detector. Here λ is the strength of the measurement. The limit $\lambda \rightarrow 0$ corresponds to a weak measurement. In this limit, the noise increases, and thus also the uncertainty of the measurement. Here, no information can be extracted from the measurements and feedback is applied randomly fifty percent of the times. The limit $\lambda \rightarrow \infty$ corresponds to a projective measurement, where the noise vanishes, eliminating all uncertainty.

Here we focus on the regime $\gamma \gg \max\{g, \Gamma_{kl}^\pm\}$, where the detector is much faster than the dynamics of the system. This is beneficial for entanglement production as the detector never lags behind the system, reducing feedback mistakes due to detector delay. However, as the ratio between γ and λ determines the magnitude of the noise, feedback mistakes due to noise can still occur. For a fast detector ($\gamma \gg \max\{g, \Gamma_{kl}^\pm\}$), equation (7) can be reduced to a Markovian master equation for the system alone [17]. It is given by

$$\partial_t \hat{\rho}_t = \mathcal{L}_{fb} \hat{\rho}_t, \tag{8}$$

where the feedback-controlled dynamics are described by \mathcal{L}_{fb} . In appendix A.1, we detail the derivation of this equation, where we also give the general form of \mathcal{L}_{fb} . In section 4.1, where we study ideal conditions, we present a simple representation of \mathcal{L}_{fb} .

4. Results

4.1. Ideal operation

To optimize the entanglement generation in the system, it is useful to study limiting cases of various parameters. Here we study two such limits, and refer to these as ideal operation conditions—this is motivated in figures 4 and 5 below. The first limit is $T_C \rightarrow 0$, ensuring that the cold bath cannot thermally excite the cold qubit ($\Gamma_{Cl}^+ \rightarrow 0$), and thus reduces the population of $|11\rangle$. The second limit is $\lambda \rightarrow \infty$, which is physically motivated as the measurement is backaction-free. Therefore, this limit is not detrimental for the entanglement generation. Additionally, this limit completely suppresses the noise in the detector, such that feedback is always applied correctly.

Under these limits, the Liouville superoperator in equation (8) can, by vectorizing the nonzero elements of the density matrix as $\hat{\varrho} = (\varrho_{00}, \varrho_{01}, \varrho_{10}, \varrho_{11}, \alpha, \alpha^*)^T$, be written in matrix representation as

$$\mathcal{L}_{fb} = \begin{bmatrix} -\Gamma_{H0}^+ & 0 & \Gamma_{C0}^- & 0 & 0 & 0 \\ \Gamma_{H0}^+ & 0 & 0 & \Gamma_{Cl}^- & ig & -ig \\ 0 & 0 & -\Gamma_{C0}^- & \Gamma_{H1}^- & -ig & ig \\ 0 & 0 & 0 & -\Gamma_{Cl}^- - \Gamma_{H1}^- & 0 & 0 \\ 0 & ig & -ig & 0 & -\frac{\Gamma_{C0}^-}{2} & 0 \\ 0 & -ig & ig & 0 & 0 & -\frac{\Gamma_{C0}^-}{2} \end{bmatrix}. \quad (9)$$

Under ideal operation conditions, excitations are unidirectionally transported from the hot to cold reservoir. This is beneficial for entanglement production as an excitation in the hot qubit only can interact coherently with the cold qubit, thus reducing the population of $|00\rangle$. Additionally, we note that the doubly excited state $|11\rangle$ is decoupled from the remaining states, and will thus vanish in the stationary state.

The null-space of \mathcal{L}_{fb} corresponds to the stationary state of equation (8) and provides the following stationary concurrence of the system (see appendix A.2)

$$\mathcal{C}(\hat{\varrho}_\infty) = \frac{4g\Gamma_{C0}^-\Gamma_{H0}^+}{4g^2(\Gamma_{C0}^- + 2\Gamma_{H0}^+) + (\Gamma_{C0}^-)^2\Gamma_{H0}^+}. \quad (10)$$

The concurrence attains its maximum $\mathcal{C}(\hat{\varrho}_\infty) = 1/\sqrt{2} \approx 0.71$ when $\Gamma_{H0}^+ \gg \Gamma_{C0}^-$ and $\Gamma_{C0}^-/g = 2\sqrt{2}$, thus significantly increasing the concurrence obtained in the absence of measurement and feedback [4]. The condition $\Gamma_{H0}^+ \gg \Gamma_{C0}^-$ ensures that an excitation quickly enters the system via the hot bath when the system occupies $|00\rangle$. This increases the population in the subspace $\{|01\rangle, |10\rangle\}$, favoring entanglement generation. Note that increasing g indefinitely is detrimental for the entanglement production, as it enhances Rabi oscillations in the coherently coupled subspace. Averaging over many oscillations reduces the entanglement (see equation (10)).

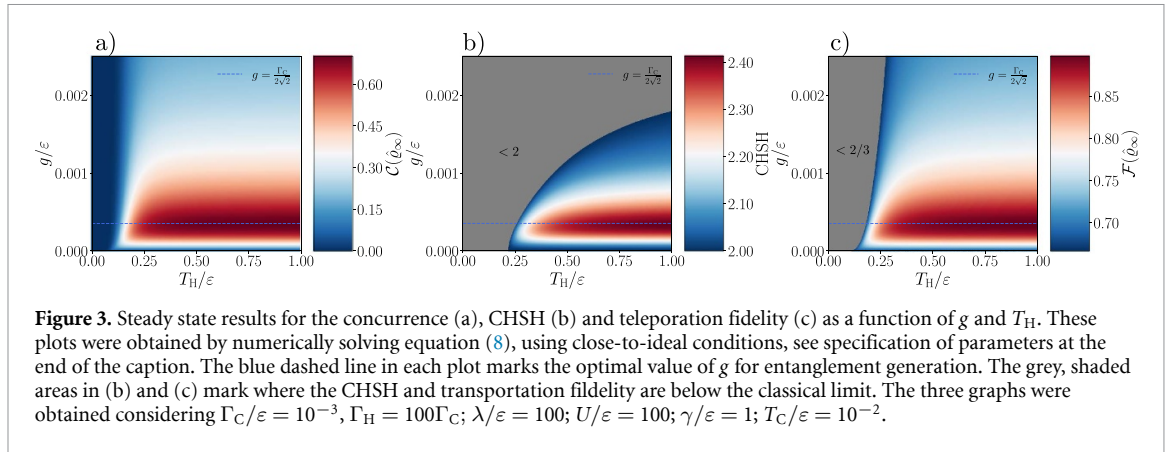
We note that the same concurrence (10) was obtained in [10] when implementing the system in a double quantum dot with $U \rightarrow \infty$ and an infinite external voltage bias across the system. For $U \rightarrow \infty$, $|11\rangle$ cannot be occupied, and with infinite bias, electrons can only move unidirectionally towards the bath with lowest chemical potential. Thus, in the absence of measurements and feedback, the system autonomously evolves according to equation (9), explaining why our result coincide with [10]. However, note that our result is valid for finite U , even for non-interacting particles ($U = 0$).

As excitations are transported from the hot to cold bath, heat will flow through the system. Due to the coherent interaction between the qubits, a nonzero heat current indicates the presence of coherence in the system, and is necessary for entanglement production [4]. Under ideal operation conditions, the heat current is given by (derivation in appendix A.5)

$$\dot{Q} = -\Gamma_{C0}^- \text{tr} \{ \hat{H}D [\hat{J}_{C0}] \hat{\varrho}_\infty \} = \varepsilon g \mathcal{C}(\hat{\varrho}_\infty), \quad (11)$$

with $\hat{\varrho}_\infty = \int dD \hat{\varrho}_\infty(D)$. Note that the derivation in section A.5 is valid in the regime of no net-power output. This is a valid regime to consider whenever no potential bias is applied to the system, which is the case in this paper. We stress that equation (11) is independent of particle type. The relation implies that the concurrence can be directly inferred by measuring the heat current, and does not require quantum state tomography. This implies that the heat current is an entanglement witness, where a nonzero current indicate the presence of entanglement. However, it is important to notice that this result is only valid in the regime of a strong interqubit interaction U , or for engines operating within the ideal operation conditions described above.

While the concurrence indicates whether a state is entangled or not, it does not provide any information on how useful the entanglement is for quantum information processing. Therefore, it is useful, as a



complement to the concurrence, to evaluate if an entangled state is able to perform non-classical tasks in quantum information processing. To this end, we evaluate whether the generated entanglement can violate the CHSH inequality and perform quantum teleportation [6].

For the state in equation (4), the CHSH inequality may be expressed as $\text{CHSH} \leq 2$, where [6, 10]

$$\text{CHSH} = 2\sqrt{8\alpha^2 + (2\Delta - 1)^2} - \min\{4\alpha^2, (2\Delta - 1)^2\}, \quad (12)$$

with $\Delta \equiv \varrho_{01} + \varrho_{10}$. If $\text{CHSH} > 2$, the system state shows Bell nonlocality. For maximally entangled states $\text{CHSH} = 2\sqrt{2}$. At maximum concurrence for ideal operation conditions, $\text{CHSH} = \sqrt{6} \approx 2.45$. In fact, this is the maximum value the CHSH can attain under the feedback protocol, see appendix A.4.

To quantify how well $\hat{\rho}_\infty$ can perform quantum teleportation, we calculate the teleportation fidelity $\mathcal{F}(\hat{\rho}_\infty) = [1 + 2F(\hat{\rho}_\infty)]/3$, where $F(\hat{\rho}_\infty)$ is the singlet tinfraction for a two qubit system $\hat{\rho}_\infty$ (see appendix A.3) [25]. For states taking the form of equation (4), the singlet fraction is expressed as [6]

$$F(\hat{\rho}) = \begin{cases} \alpha + \frac{\Delta}{2} & \text{if } (1 + 2\alpha - 2\Delta) \leq 0 \\ \max\{\alpha + \frac{\Delta}{2}, \frac{1-\Delta}{2}\} & \text{otherwise} \end{cases}. \quad (13)$$

For a maximally entangled state, $\mathcal{F}(\hat{\rho}_\infty) = 1$. A classical implementation of the protocol can at best achieve $\mathcal{F} = 2/3$ [25], implying that the state contains non-trivial levels of entanglement when $F(\hat{\rho}_\infty) > 1/2$. At maximum concurrence, for ideal operation conditions, we obtain $\mathcal{F}(\hat{\rho}_\infty) = (4 + \sqrt{2})/6 \approx 0.9$. Note that this is the maximum fidelity that can be achieved with the feedback protocol, see appendix A.3. In figure 3, we plot the concurrence, CHSH, and teleportation fidelity, using close-to-ideal conditions.

4.2. Beyond ideal operation

Now we discuss the entanglement production when relaxing the ideal operation conditions. The ideal conditions are relaxed one by one, such that the role of each parameter can be understood carefully. We also discuss the effect of the last term of the Hamiltonian in equation (1). We focus on investigating how the concurrence depends on the system parameters. For a similar analysis of CHSH and the quantum teleportation fidelity, the reader is referred to appendix A.6. However, such an analysis does not provide any additional information compared to the concurrence. The figures presented in this section focus on fermionic reservoirs (see equation (3)), but a similar behavior is observed for bosonic reservoirs, see appendix A.6.

By relaxing $\lambda \rightarrow \infty$, the detector becomes noisy—recall that the magnitude of the noise is determined by λ/γ , as discussed under equation (7). A noisy detector introduces feedback mistakes. That is, the coupling to the hot bath can remain open even though $|01\rangle$ or $|10\rangle$ are occupied. This increases the populations of $|00\rangle$ and $|11\rangle$, because an excitation in the hot qubit can re-enter the hot bath when $|01\rangle$ is occupied, or enter the hot qubit when $|10\rangle$ is occupied. This reduces the entanglement in the system, see figures 4 and 5.

Additionally, the figures illustrate that it is favorable to use $\lambda \gg \gamma$, as seen in the previous subsection. We also note that feedback mistakes increase the decoherence induced by the hot bath, as the coupling to the hot bath can remain open even though $|01\rangle$ or $|10\rangle$ are occupied, see equation (A.8) in appendix A.2. We remind the reader that the measured observable is backaction-free, such that the strength of the measurement does not destroy the entanglement of the system.

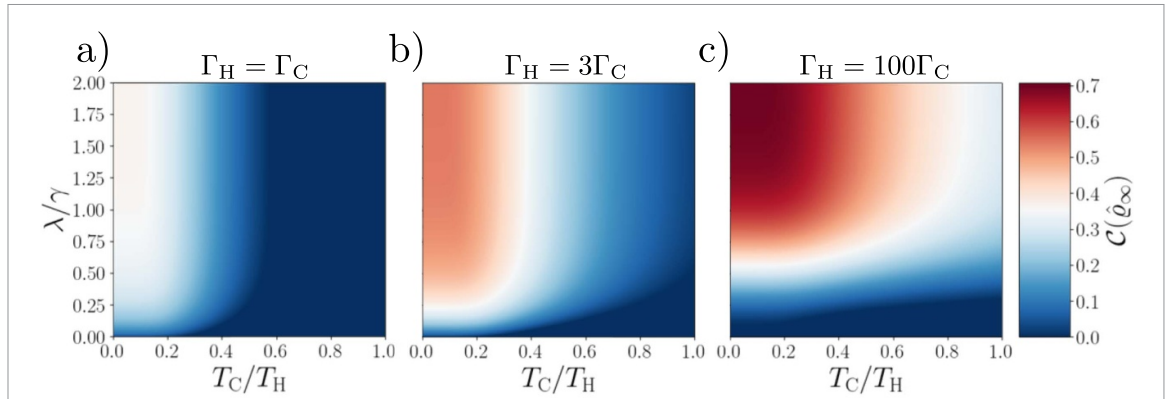


Figure 4. Steady state concurrence as a function of measurement strength λ and temperature of the cold reservoir T_C for three values of Γ_H (see top of graphs). Here we focus on fermionic reservoirs (similar results are obtained for bosons, see appendix A.6). All plots indicate that the concurrence decreases with the measurement strength λ , as feedback mistakes become prominent. By increasing T_C , the cold qubit can be thermally excited, increasing the population of $|11\rangle$ and thus reducing the concurrence. For $\Gamma_H \gg \Gamma_C$, the hot bath quickly provides an excitation to the system when occupying $|00\rangle$, reducing the population of this state and favors entanglement generation. All of the above plots were obtained considering $U/\varepsilon = 0$, $\Gamma_C/\varepsilon = 10^{-3}$, $\Gamma_C/g = 2\sqrt{2}$ and $T_H/\varepsilon = 1$, $\gamma/\varepsilon = 1$.

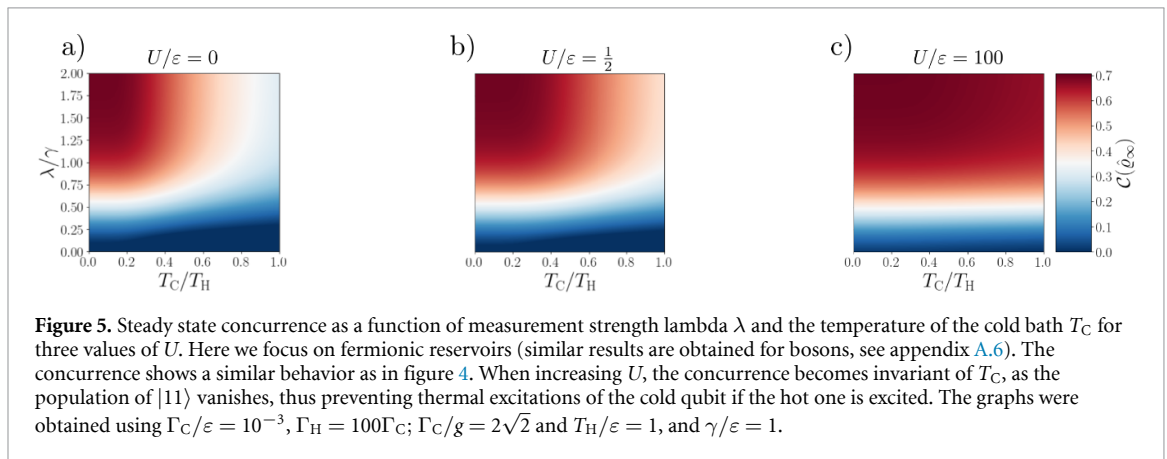


Figure 5. Steady state concurrence as a function of measurement strength λ and the temperature of the cold bath T_C for three values of U . Here we focus on fermionic reservoirs (similar results are obtained for bosons, see appendix A.6). The concurrence shows a similar behavior as in figure 4. When increasing U , the concurrence becomes invariant of T_C , as the population of $|11\rangle$ vanishes, thus preventing thermal excitations of the cold qubit if the hot one is excited. The graphs were obtained using $\Gamma_C/\varepsilon = 10^{-3}$, $\Gamma_H = 100\Gamma_C$; $\Gamma_C/g = 2\sqrt{2}$ and $T_H/\varepsilon = 1$, and $\gamma/\varepsilon = 1$.

For $T_C \neq 0$, $\Gamma_{Cl}^+ \neq 0$, enabling thermal excitations of the cold qubit. The population of $|11\rangle$ thus increases as the cold qubit may be excited when occupying $|01\rangle$, decreasing the entanglement. We also note that $\Gamma_{Cl}^+ \neq 0$ results in bath-induced decoherence, deteriorating the entanglement, see equation (A.8) in appendix A.2. The overall effect of $T_C \neq 0$ is thus to decrease the entanglement—this is illustrated in figures 4 and 5.

Below equation (10), we noted that $\Gamma_{H0}^+ \gg \Gamma_{C0}^-$ was favorable for entanglement generation as the population in the subspace $\{|01\rangle, |10\rangle\}$ was increased. Relaxing this condition increases the population of $|00\rangle$, as it takes longer time for an excitation to enter the hot qubit when the system occupies $|00\rangle$. Similarly, when Γ_C^- is small, the population of $|00\rangle$ decreases, as an excitation stays longer in the system, favoring coherent interaction between the qubits. Thus, relaxing the condition $\Gamma_{H0}^+ \gg \Gamma_{C0}^-$ decreases the entanglement as illustrated in figure 4.

So far, we have not made any assumptions about the interaction U in the Hamiltonian (1). In fact, under ideal operation conditions ($T_C = 0$ and $\lambda \rightarrow \infty$), the interaction does not play any role for the stationary state of the system as the population of $|11\rangle$ vanishes, see equation (9). However, when relaxing one, or both, of the ideal conditions, U affects the stationary state as the population of $|11\rangle$ becomes nonzero. In figure 5, we illustrate the effect of U on the concurrence. We see that the concurrence is dependent on T_C for non-interacting excitations ($U = 0$), while a large U eliminates this dependence. This happens because the population of $|11\rangle$ vanishes for large U , preventing thermal excitations when $|01\rangle$ is occupied.

For ideal conditions, we found that the heat current is proportional to the concurrence. In fact, this proportionality holds true when relaxing the ideal conditions, but taking the limit $U \rightarrow \infty$, where the population of $|11\rangle$ vanishes, see appendix A.2. For finite U , this proportionality does not hold true anymore. This agrees with the results derived in [5], where it was found that the qubits, in the absence of feedback, are entangled if the heat current surpasses a critical heat current. In particular, we show that the developed

protocol is capable of retrieving steady states with vanishing $|11\rangle$ population. Through these we recover a specific variation of the results obtained in [5]. In these cases, the absence of $|11\rangle$ population, allows us to indicate non zero heat currents as entanglement witnesses.

5. Conclusion and outlook

In this paper, we introduced a continuous feedback protocol aiming to increase the stationary entanglement production of a quantum thermal machine consisting of two coherently interacting qubits, incoherently coupled to two thermal reservoirs. In the absence of feedback, it was shown in [4] that a temperature gradient between the reservoirs could weakly entangle the qubits. The feedback protocol only makes use of local operations, measuring the parity observable of the qubits and controlling the coupling to the warmer environment. Our investigation shows that the protocol increases the stationary entanglement production. In particular, we identified an ideal operation regime where the entanglement significantly increases. This involved putting the temperature of the colder bath to zero and performing projective measurements. In this regime, we find that the heat current across the system is proportional to the concurrence. This implies that a nonzero heat current acts as an entanglement witness. In addition, we investigated the operational usefulness of the entanglement, and found that the entanglement is capable of violating the CHSH inequality and performing quantum teleportation, which was not possible in the absence of the feedback protocol. We additionally studied the entanglement production under non-ideal conditions. Decreasing the strength of the measurement (performing nonprojective measurements) induces mistakes in the feedback, lowering the entanglement production. Similarly, the entanglement decreases when the temperature of the cold bath is nonzero, as the cold qubit can be thermally excited.

Extensions of the protocol involves, e.g. heralding [7], which has the potential of generating maximally entangled states, and extensions to multipartite systems. Finally, we note that several experimental platforms are available for realizing the protocol. Among these, semiconductor quantum dots and superconducting qubits are promising candidates.

Data availability statement

All data that support the findings of this study are included within the article (and any supplementary files).

Acknowledgments

We thank Patrick P Potts for fruitful discussions. P S and B A A were supported by the Swedish Research Council, Grant No. 2018-03921. P B is supported by grant number FQXi Grant Number: FQXi-IAF19-07 from the Foundational Questions Institute Fund, a donor advised fund of Silicon Valley Community Foundation. P B also acknowledges funding from the European Research Council (Consolidator Grant ‘Cocoquest’ 101043705. G F D acknowledges the Wallenberg Center for Quantum Technology (WACQT) for financial support via the EDU-WACQT program funded by Marianne and Marcus Wallenberg Foundation. A T is supported by the Wenner-Gren Foundation and by the Knut and Alice Wallenberg Foundation through the Wallenberg Center for Quantum Technology (WACQT).

Appendix

A.1. Derivation of equation (8)

In this section, we provide a derivation for equation (8). The method for this derivation was first presented in [17]. We begin by writing equation (7) as

$$\partial_t \hat{\rho}_t(D) = \mathcal{L}(D) \hat{\rho}_t(D) + \mathcal{F}(D) \hat{\rho}_t(D), \quad (\text{A.1})$$

where we introduced the superoperator

$$\mathcal{F}(D) = -\gamma \partial_D \mathcal{A}(D) + \frac{\gamma^2}{8\lambda} \partial_D^2. \quad (\text{A.2})$$

We are interested in the fast detector regime where $\gamma \gg \max\{g, \Gamma_{kl}^\pm\}$. To this end, we can expand the density matrix $\hat{\rho}_t(D)$ in powers of $1/\gamma$. Following the procedure of [17] (see section II in the supplemental material of [17]), we find, to zeroth order in $1/\gamma$, that

$$\hat{\rho}_t(D) = \sum_{aa'} \pi_{aa'}(D) \mathcal{V}_{aa'} \hat{\rho}_t, \quad (\text{A.3})$$

where $\hat{\varrho}_t = \int dD \hat{\varrho}_t(D)$ is the state of the system, $\mathcal{V}_{aa'} \hat{\varrho} = \langle a | \hat{\varrho} | a' \rangle | a \rangle \langle a' |$, with $| a \rangle$ being the eigenstates of the observable $\hat{A} = \hat{\sigma}_z \otimes \hat{\sigma}_z$, and

$$\pi_{aa'}(D) = \sqrt{\frac{4\lambda}{\pi\gamma}} e^{-\frac{4\lambda}{\gamma} [D - (\xi_a + \xi_{a'})/2]^2}, \quad (\text{A.4})$$

with ξ_a being the eigenvalues corresponding to the eigenstate $| a \rangle$. By plugging equation (A.3) into equation (A.1) and integrating over D , we find equation (8) with

$$\mathcal{L}_{\text{fb}} = \mathcal{L}[(1 - \eta)(\mathcal{V}_{00,00} + \mathcal{V}_{11,11}) + \eta(1 - \mathcal{V}_{00,00} - \mathcal{V}_{11,11})] \quad (\text{A.5})$$

$$+ \tilde{\mathcal{L}}[\eta(\mathcal{V}_{00,00} + \mathcal{V}_{11,11}) + (1 - \eta)(1 - \mathcal{V}_{00,00} - \mathcal{V}_{11,11})], \quad (\text{A.6})$$

where we introduced the feedback error probability

$$\eta = \frac{1}{2} \left[1 - \text{erf} \left(2\sqrt{\frac{\lambda}{\gamma}} \right) \right]. \quad (\text{A.7})$$

By vectorizing the density matrix as $\hat{\varrho}_t = (\varrho_{00}, \varrho_{01}, \varrho_{10}, \varrho_{11}, \alpha, \alpha^*)^T$, \mathcal{L}_{fb} can be written in matrix form as

$$\mathcal{L}_{\text{fb}} = \begin{bmatrix} -\Gamma_{\text{C0}}^+ - \Gamma_{\text{H0}}^+(1 - \eta) & \eta\Gamma_{\text{H0}}^- & \Gamma_{\text{C0}}^- & 0 & 0 & 0 \\ \Gamma_{\text{H0}}^+(1 - \eta) & -\Gamma_{\text{C1}}^+ - \eta\Gamma_{\text{H0}}^- & 0 & \Gamma_{\text{C1}}^- & ig & -ig \\ \Gamma_{\text{C0}}^+ & 0 & -\Gamma_{\text{C0}}^- & \Gamma_{\text{H1}}^-(1 - \eta) & -ig & ig \\ 0 & \Gamma_{\text{C1}}^+ & \eta & -\Gamma_{\text{C1}}^- - \Gamma_{\text{H1}}^-(1 - \eta) & 0 & 0 \\ 0 & ig & -ig & 0 & -\frac{1}{2}[\Gamma_{\text{C1}}^+ + \eta\Gamma_{\text{H0}}^- + \Gamma_{\text{C0}}^-] & 0 \\ 0 & -ig & ig & 0 & 0 & -\frac{1}{2}[\Gamma_{\text{C1}}^+ + \eta\Gamma_{\text{H0}}^- + \Gamma_{\text{C0}}^-] \end{bmatrix}. \quad (\text{A.8})$$

A.2. Steady state solutions to equation (8)

In this section, we provide the stationary solution to equation (8) for ideal operation conditions ($\lambda \rightarrow \infty$ and $T_{\text{C}} \rightarrow 0$) and when taking the limit $U \rightarrow \infty$. We do not present the general stationary state of equation (A.8) as the expressions are too long.

The ideal operation conditions are equivalent to $\eta \rightarrow 0$ (feedback always applied correctly) and $\Gamma_{\text{C1}}^+ \rightarrow 0$. Under these limits, equation (A.8) simplifies to

$$\mathcal{L}_{\text{fb}} = \begin{bmatrix} -\Gamma_{\text{H0}}^+ & 0 & \Gamma_{\text{C0}}^- & 0 & 0 & 0 \\ \Gamma_{\text{H0}}^+ & 0 & 0 & \Gamma_{\text{C1}}^- & ig & -ig \\ 0 & 0 & -\Gamma_{\text{C0}}^- & \Gamma_{\text{H1}}^- & -ig & ig \\ 0 & 0 & 0 & -\Gamma_{\text{C1}}^- - \Gamma_{\text{H1}}^- & 0 & 0 \\ 0 & ig & -ig & 0 & -\frac{1}{2}\Gamma_{\text{C0}}^- & 0 \\ 0 & -ig & ig & 0 & 0 & -\frac{1}{2}\Gamma_{\text{C0}}^- \end{bmatrix}. \quad (\text{A.9})$$

The stationary state corresponds to the nullspace of \mathcal{L}_{fb} , and is given by

$$\hat{\varrho}_{\infty} = \frac{1}{\mathcal{N}} \begin{bmatrix} 4g^2\Gamma_{\text{C0}}^- & 0 & 0 & 0 \\ 0 & (4g^2 + \Gamma_{\text{C0}}^-^2)\Gamma_{\text{H0}}^+ & 2ig\Gamma_{\text{C0}}^-\Gamma_{\text{H0}}^+ & 0 \\ 0 & -2ig\Gamma_{\text{C0}}^-\Gamma_{\text{H0}}^+ & 4g^2\Gamma_{\text{H0}}^+ & 0 \\ 0 & 0 & 0 & 0 \end{bmatrix}, \quad (\text{A.10})$$

where $\mathcal{N} = (\Gamma_{\text{C0}}^-)^2\Gamma_{\text{H0}}^+ + 4g^2(\Gamma_{\text{C0}}^- + 2\Gamma_{\text{H0}}^+)$ is a normalization constant. We note that the population of the doubly excited state vanishes, even though we did not make any assumptions on U . By identifying α , ϱ_{00} and ϱ_{11} (equation (4)), and using equation (5), we get the expression for concurrence given in equation (10). We also stress that we have made no assumptions whether the baths are fermionic or bosonic, the results are valid for both.

We now look at the limit $U \rightarrow \infty$, corresponding to $\Gamma_{kl}^+ \rightarrow 0$. Equation (A.8) simplifies to

$$\mathcal{L}_{fb} = \begin{bmatrix} -\Gamma_{C0}^+ - \Gamma_{H0}^+(1-\eta) & \eta\Gamma_{H0}^- & \Gamma_{C0}^- & 0 & 0 & 0 \\ \Gamma_{H0}^+(1-\eta) & -\eta\Gamma_{H0}^- & 0 & \Gamma_{C1}^- & ig & -ig \\ \Gamma_{C0}^+ & 0 & -\Gamma_{C0}^- & \Gamma_{H1}^-(1-\eta) & -ig & ig \\ 0 & 0 & 0 & -\Gamma_{C1}^- - \Gamma_{H1}^-(1-\eta) & 0 & 0 \\ 0 & ig & -ig & 0 & -\frac{1}{2}[\eta\Gamma_{H0}^- + \Gamma_{C0}^-] & 0 \\ 0 & -ig & ig & 0 & 0 & -\frac{1}{2}[\eta\Gamma_{H0}^- + \Gamma_{C0}^-] \end{bmatrix}. \quad (A.11)$$

Note that all rates accompanied by $1 - \eta$ correspond to transitions when applying feedback correctly, and all rates with an η correspond to transitions when feedback is applied wrongly. Similar to the ideal operation conditions, $|11\rangle$ is decoupled from the remaining states in the stationary limit. Here we write the stationary state as

$$\hat{\rho}_\infty = \frac{1}{\tilde{\mathcal{N}}} \begin{bmatrix} \varrho'_{00} & 0 & 0 & 0 \\ 0 & \varrho'_{01} & \alpha' & 0 \\ 0 & \alpha'^* & \varrho'_{10} & 0 \\ 0 & 0 & 0 & \varrho'_{11} \end{bmatrix}, \quad (A.12)$$

where $\tilde{\mathcal{N}}$ is a normalization constant. The matrix elements and normalization constant are given by

$$\varrho'_{00} = (\Gamma_{C0}^- + \eta\Gamma_{H0}^-) (\eta\Gamma_{C0}^-\Gamma_{H0}^- + 4g^2), \quad (A.13)$$

$$\varrho'_{01} = 4g^2\Gamma_{C0}^+ + (1-\eta)\Gamma_{H0}^+ [\Gamma_{C0}^{-2} + \eta\Gamma_{C0}^-\Gamma_{H0}^- + 4g^2], \quad (A.14)$$

$$\varrho'_{10} = 4(1-\eta)g^2\Gamma_{H0}^+ + \Gamma_{C0}^+ [\eta\Gamma_{H0}^- (\Gamma_{C0}^- + \eta\Gamma_{H0}^-) + 4g^2], \quad (A.15)$$

$$\varrho'_{11} = 0, \quad (A.16)$$

$$\alpha' = 2ig [(1-\eta)\Gamma_{C0}^-\Gamma_{H0}^+ - \eta\Gamma_{C0}^+\Gamma_{H0}^-], \quad (A.17)$$

$$\tilde{\mathcal{N}} = 8g^2 [\Gamma_{C0}^+ + (1-\eta)\Gamma_{H0}^+] + \Gamma_{C0}^- [\eta\Gamma_{H0}^- [\Gamma_{C0}^+ + \eta\Gamma_{H0}^- + (1-\eta)\Gamma_{H0}^+] + 4g^2] \quad (A.18)$$

$$+ \eta^2\Gamma_{C0}^+\Gamma_{H0}^{-2} + \Gamma_{C0}^{-2} [\eta\Gamma_{H0}^- + (1-\eta)\Gamma_{H0}^+] + 4\eta g^2\Gamma_{H0}^-. \quad (A.19)$$

A.3. Optimizing teleportation fidelity

In this section, we show that the teleportation fidelity is maximized for the same parameters that maximizes the concurrence in section 4. To do so, we work with the optimal operation conditions $\lambda \rightarrow \infty$ and $T_C \rightarrow 0$. To carry out an optimization for the teleportation fidelity, we follow a standard optimization scheme and consider the gradient $\nabla \equiv (\partial_g, \partial_{\Gamma_{C0}^-}, \partial_{\Gamma_{H0}^+})^T$ of equation (13) for a general steady state of the Liouvillian in equation (A.9). Doing so leads us to the expressions

$$\nabla F(\hat{\rho}_\infty) = \begin{cases} \mathcal{N} \begin{pmatrix} 2\Gamma_{C0}^-\Gamma_{H0}^+ [-2\Gamma_{C0}^-g(\Gamma_{C0}^- + 2g) + (\Gamma_{C0}^{-2} - 8g^2)\Gamma_{H0}^+] \\ 2g\Gamma_{H0}^+ (\Gamma_{C0}^{-2} - 8g^2)(g - \Gamma_{H0}^+) \\ 2g^2\Gamma_{C0}^- (\Gamma_{C0}^{-2} + 4g\Gamma_{C0}^- + 8g^2) \end{pmatrix} & \text{if } 1 + 2\alpha - 2\Delta \leq 0 \\ -\mathcal{N} \begin{pmatrix} -4g\Gamma_{C0}^{-3}\Gamma_{H0}^+ \\ 2g^2\Gamma_{H0}^+ (\Gamma_{C0}^{-2} - 8g^2) \\ 2g^2\Gamma_{C0}^- (\Gamma_{C0}^{-2} + 8g^2) \end{pmatrix} & \text{otherwise} \end{cases} \quad (A.20)$$

where $\mathcal{N} = (\Gamma_{C0}^{-2}\Gamma_{H0}^+ + 4g^2\Gamma_{C0}^- + 8g^2\Gamma_{H0}^+)^{-2}$. Using equation (A.20) we find that regardless of whether or not $1 + 2\alpha - \Delta \leq 0$, optimal fidelity is obtained for $g = \Gamma_{C0}^-/2\sqrt{2}$, which is the same result obtained when optimizing the system concurrence. By inserting this value of g in equation (13), we obtain

$$\mathcal{F}(\hat{\rho}_\infty) = \frac{1}{3} \left(1 + \frac{(4 + 2\sqrt{2})\Gamma_{H0}^+}{\Gamma_{C0}^- + 4\Gamma_{H0}^+} \right), \quad (A.21)$$

which is a monotonic function in Γ_{H0}^+ . Thus, considering $\Gamma_{H0}^+ \gg \Gamma_{C0}^-$ we obtain the optimal solution $\mathcal{F}(\hat{\rho}_\infty) = (4 + \sqrt{2})/6 \approx 0.90$ that we presented in section 4.

A.4. Optimizing CHSH

In this section, we show that the CHSH is maximized for the same parameters that maximizes the concurrence in section 4. As in the case with fidelity, we carry out this optimization procedure by analytically obtaining an expression for the gradient $\nabla \equiv (\partial_g, \partial_{\Gamma_{\text{Co}}^-}, \partial_{\Gamma_{\text{Ho}}^+})$ of equation (12) for ideal operation conditions. This is carried out by separating the cases in which $4\alpha^2 - (2\Delta - 1)^2 \leq 0$ from all others. In the case where $4\alpha^2 - (2\Delta - 1)^2 > 0$, the gradient of equation (12) evaluated for the steady state of equation (9) returns

$$\nabla \text{CHSH} = \begin{pmatrix} g\Gamma_{\text{Ho}}^+ \Gamma_{\text{Co}}^{-2} (64\sqrt{2}g^2 - 8\sqrt{2}\Gamma_{\text{Co}}^{-2}) \\ g^2\Gamma_{\text{Ho}}^+ \Gamma_{\text{Co}}^- (8\sqrt{2}\Gamma_{\text{Co}}^{-2}\Gamma_{\text{Ho}}^+ - 32\sqrt{2}\Gamma_{\text{Co}}^-g^2 - 64\sqrt{2}g^2\Gamma_{\text{Ho}}^+) \\ 32\sqrt{2} \left(\frac{\Gamma_{\text{Co}}^{-4} g^3 \Gamma_{\text{Ho}}^6}{\sqrt{\Gamma_{\text{Co}}^{-2}\Gamma_{\text{Ho}}^+ + 4\Gamma_{\text{Co}}^-g^2 + 8g^2\Gamma_{\text{Ho}}^+}} \right) \end{pmatrix}. \quad (\text{A.22})$$

Setting equation (A.22) to zero and solving for g , Γ_{Co}^- and Γ_{Ho}^+ returns a maximum value of $\text{CHSH} = 2$ at $g = \frac{\Gamma_{\text{Co}}^- \sqrt{\Gamma_{\text{Ho}}^+}}{\sqrt{4\Gamma_{\text{Co}}^- + 8\Gamma_{\text{Ho}}^+}}$. However, if we instead carry out the optimization procedure, by considering the gradient of equation (12) for $4\alpha^2 - (2\Delta - 1)^2 \leq 0$, we obtain

$$\nabla \text{CHSH} = \begin{pmatrix} \frac{g^2\Gamma_{\text{Ho}}^+ (\Gamma_{\text{Co}}^{-3} (-64g^2 - 32\Gamma_{\text{Ho}}^+) + 16\Gamma_{\text{Co}}^{-4}\Gamma_{\text{Ho}}^+ + \Gamma_{\text{Co}}^- (256g^2\Gamma_{\text{Ho}}^+ + 512g^4) - 1024g^4\Gamma_{\text{Ho}}^+)}{(\Gamma_{\text{Co}}^{-2}\Gamma_{\text{Ho}}^+ + 4\Gamma_{\text{Co}}^-g^2 + 8g^2\Gamma_{\text{Ho}}^+)^2 \sqrt{\Gamma_{\text{Co}}^{-2} (32g^2\Gamma_{\text{Ho}}^+ + 16g^4) - 8\Gamma_{\text{Co}}^{-3}g^2\Gamma_{\text{Ho}}^+ + \Gamma_{\text{Co}}^{-4}\Gamma_{\text{Ho}}^+ - 64\Gamma_{\text{Co}}^-g^4\Gamma_{\text{Ho}}^+ + 64g^4\Gamma_{\text{Ho}}^+}} \\ \frac{\Gamma_{\text{Co}}^- g\Gamma_{\text{Ho}}^+ (\Gamma_{\text{Co}}^{-2} (128g^2 + 32\Gamma_{\text{Ho}}^+) - 32\Gamma_{\text{Co}}^{-3}\Gamma_{\text{Ho}}^+ - 384\Gamma_{\text{Co}}^-g^2\Gamma_{\text{Ho}}^+ - 256g^2\Gamma_{\text{Ho}}^+)}{(\Gamma_{\text{Co}}^{-2}\Gamma_{\text{Ho}}^+ + 4\Gamma_{\text{Co}}^-g^2 + 8g^2\Gamma_{\text{Ho}}^+)^2 \sqrt{\Gamma_{\text{Co}}^{-2} (32g^2\Gamma_{\text{Ho}}^+ + 16g^4) - 8\Gamma_{\text{Co}}^{-3}g^2\Gamma_{\text{Ho}}^+ + \Gamma_{\text{Co}}^{-4}\Gamma_{\text{Ho}}^+ - 64\Gamma_{\text{Co}}^-g^4\Gamma_{\text{Ho}}^+ + 64g^4\Gamma_{\text{Ho}}^+}} \\ \frac{\Gamma_{\text{Co}}^- g^2 (384\Gamma_{\text{Co}}^{-2}g^2\Gamma_{\text{Ho}}^+ - 64\Gamma_{\text{Co}}^{-3}g^2 + 16\Gamma_{\text{Co}}^{-4}\Gamma_{\text{Ho}}^+ - 512\Gamma_{\text{Co}}^-g^4 + 1024g^4\Gamma_{\text{Ho}}^+)}{(\Gamma_{\text{Co}}^{-2}\Gamma_{\text{Ho}}^+ + 4\Gamma_{\text{Co}}^-g^2 + 8g^2\Gamma_{\text{Ho}}^+)^2 \sqrt{\Gamma_{\text{Co}}^{-2} (32g^2\Gamma_{\text{Ho}}^+ + 16g^4) - 8\Gamma_{\text{Co}}^{-3}g^2\Gamma_{\text{Ho}}^+ + \Gamma_{\text{Co}}^{-4}\Gamma_{\text{Ho}}^+ - 64\Gamma_{\text{Co}}^-g^4\Gamma_{\text{Ho}}^+ + 64g^4\Gamma_{\text{Ho}}^+}} \end{pmatrix}, \quad (\text{A.23})$$

which has optimal solution at $g = \frac{\Gamma_{\text{Co}}^-}{2\sqrt{2}}$ and $\Gamma_{\text{Ho}}^+ \gg \Gamma_{\text{Co}}^-$, where $\text{CHSH} = \sqrt{6} \approx 2.45$.

A.5. Heat current

Here we calculate the stationary heat current in the system. To this end, it is useful to decompose the feedback Liouvillian as $\mathcal{L}(D) = \theta(D)(\mathcal{L}_C + \mathcal{L}_H) + [1 - \theta(D)]\mathcal{L}_C$, where

$$\mathcal{L}_k = \Gamma_{k0}^+ \mathcal{D} [\hat{J}_{k0}^+] + \Gamma_{k1}^+ \mathcal{D} [\hat{J}_{k1}^+] + \Gamma_{k0}^- \mathcal{D} [\hat{J}_{k0}^-] + \Gamma_{k1}^- \mathcal{D} [\hat{J}_{k1}^-], \quad k = \text{C, H}. \quad (\text{A.24})$$

The average energy of the system is given by $E = \int dD \text{tr} \{ \hat{H} \hat{\rho}_t(D) \}$. Taking the time derivative of this gives

$$\dot{E} = - \int_{-\infty}^{\infty} dD \text{tr} \{ \hat{H} \partial_t \hat{\rho}_t(D) \} \quad (\text{A.25})$$

$$= - \int_{-\infty}^{\infty} dD \text{tr} \{ \hat{H} \mathcal{L}(D) \hat{\rho}_t(D) \} \quad (\text{A.26})$$

$$= \text{tr} \{ \hat{H} \mathcal{L}_C \hat{\rho}_t \} + \int_0^{\infty} dD \text{tr} \{ \hat{H} \mathcal{L}_H \hat{\rho}_t(D) \} \quad (\text{A.27})$$

$$= \dot{Q}_C + \dot{Q}_H, \quad (\text{A.28})$$

where the minus sign decides the sign convention, i.e. a positive sign corresponds to heat flowing into the baths, and we used that $\hat{\rho}_t = \int_{-\infty}^{\infty} dD \hat{\rho}_t(D)$, $\int_{-\infty}^{\infty} dD [-\gamma \partial_D \mathcal{A}(D) + \frac{\gamma^2}{8\lambda} \partial_D^2] \hat{\rho}_t(D) = 0$, and we introduced the following heat currents associated with the cold (C) and hot (H) baths,

$$\dot{Q}_C = -\text{tr} \{ \hat{H} \mathcal{L}_C \hat{\rho}_t \} \quad \text{and} \quad \dot{Q}_H = - \int_0^{\infty} dD \text{tr} \{ \hat{H} \mathcal{L}_H \hat{\rho}_t(D) \}. \quad (\text{A.29})$$

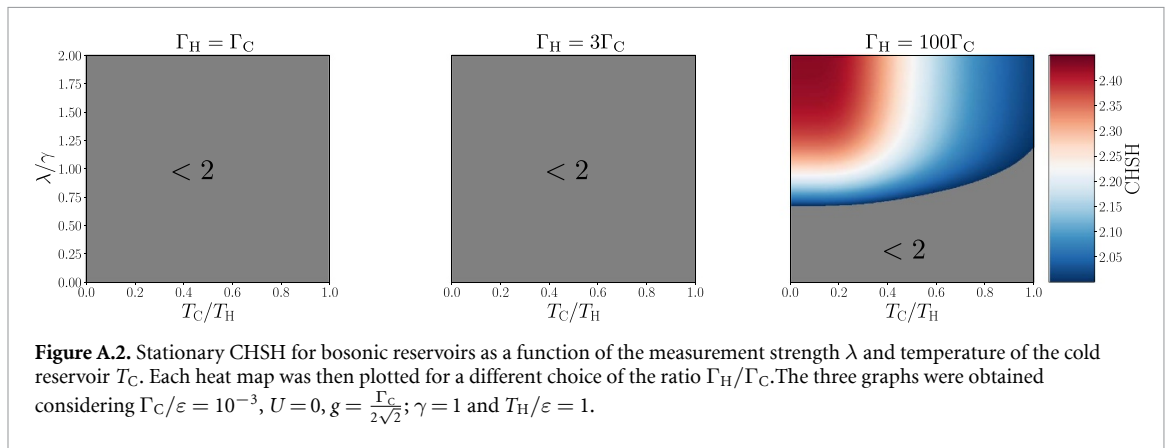
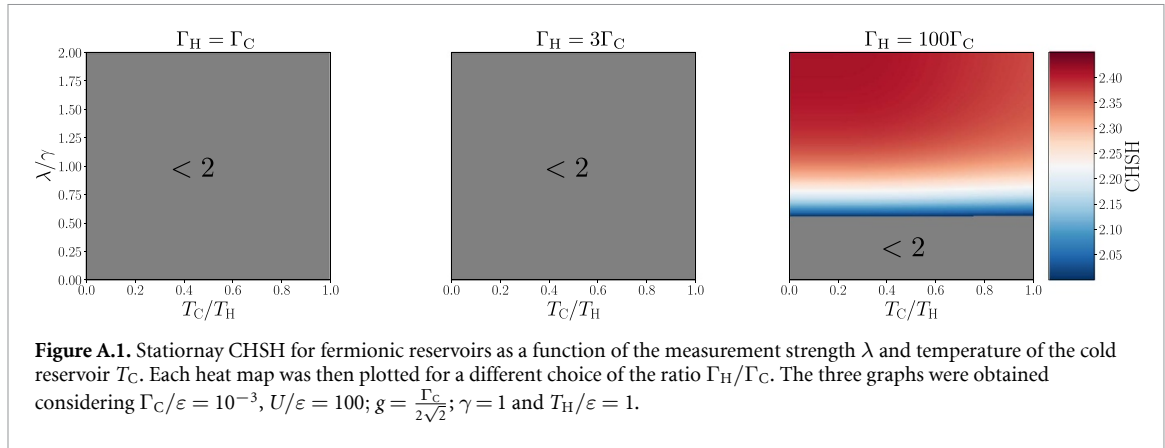
In steady state, we get the heat current $\dot{Q} = \dot{Q}_C = -\dot{Q}_H$. By using \dot{Q}_C , we get

$$\dot{Q} = (\varepsilon + U) \Gamma_{\text{C}1}^- \rho_{11} + \varepsilon \Gamma_{\text{C}0}^- \rho_{10} - \varepsilon \Gamma_{\text{C}0}^+ \rho_{00} - (\varepsilon + U) \Gamma_{\text{C}1}^+ \rho_{01}. \quad (\text{A.30})$$

Taking the limits $T_C \rightarrow 0$ ($\Gamma_{\text{C}1}^+ \rightarrow 0$) and $\lambda \rightarrow \infty$, we get, for $\gamma \gg \max\{g, \Gamma_{kl}^{\pm}\}$, that

$$\dot{Q} = \varepsilon \Gamma_{\text{C}0}^- \rho_{10} = -\Gamma_{\text{C}0}^- \text{tr} \{ \hat{H} \mathcal{D} [\hat{J}_{\text{C}0}] \hat{\rho}_{\infty} \}, \quad (\text{A.31})$$

as specified in equation (11) in the main text. By explicit calculation, using the stationary state in equation (A.10), we obtain the relation $\dot{Q} = \varepsilon g \mathcal{C}$ as specified in the main text.



We may also investigate the heat current for $U \rightarrow \infty$ ($\Gamma_{k1}^+ \rightarrow 0$). Under this limit, equation (A.30) is simplified to

$$\dot{Q} = \varepsilon (\Gamma_{C0}^- \varrho_{10} - \Gamma_{C0}^+ \varrho_{00}). \quad (\text{A.32})$$

Using the expressions from appendix A.2, we get

$$|\dot{Q}| = \frac{4g^2\varepsilon|(1-\eta)\Gamma_{C0}^-\Gamma_{H0}^+ - \eta\Gamma_{C0}^+\Gamma_{H0}^-|}{\tilde{\mathcal{N}}} = 2\varepsilon g \frac{|\alpha'|}{\tilde{\mathcal{N}}} = \varepsilon g \mathcal{C}, \quad (\text{A.33})$$

where we used equation (5). This proves that the heat current is proportional to the concurrence when $U \rightarrow \infty$.

A.6. Concurrence, CHSH, and teleportation fidelity beyond ideal operation conditions

In section 4.2 we studied the steady state concurrence of the system outside the regime of ideal operation conditions, see section 4. In this section, we study CHSH and the teleportation fidelity for both bosonic and fermionic reservoirs beyond the ideal operation conditions. For the bosons, we only consider $U = 0$, as the reservoirs naturally would consist of photons or phonons, and thereby, do not carry charge.

Figure A.1 shows CHSH of the fermionic system as a function of λ and T_C for different choices of Γ_H . Similarly to what we found in section 4, from figure A.1 we see that increasing the coupling to the hot reservoir results in higher values of CHSH. However, a violation of Bell's inequality is achieved only in the limit $\Gamma_H \gg \Gamma_C$. On the other hand, if we compare the results obtained for the fermionic system with the ones obtained for the bosonic engine (see figure A.2), we notice that within similar parameter regimes the bosonic engine is capable of producing higher CHSH values. This is due to the difference between the Bose–Einstein and Fermi–Dirac distributions, which allows the bosonic engine to produce higher heat currents, see equation (3). However, a stronger coupling to the hot reservoir is still required in order to violate Bell's inequality.

In figure A.3 we instead study the CHSH for the fermionic engine as a function of λ and T_C for different choices of interqubit interaction strength U . From these maps we see that for $U/\varepsilon = 0$ we recover the optimal CHSH value when within the limit $\lambda \rightarrow \infty$ and $T_C \rightarrow 0$. Furthermore, increasing the value of U allows for

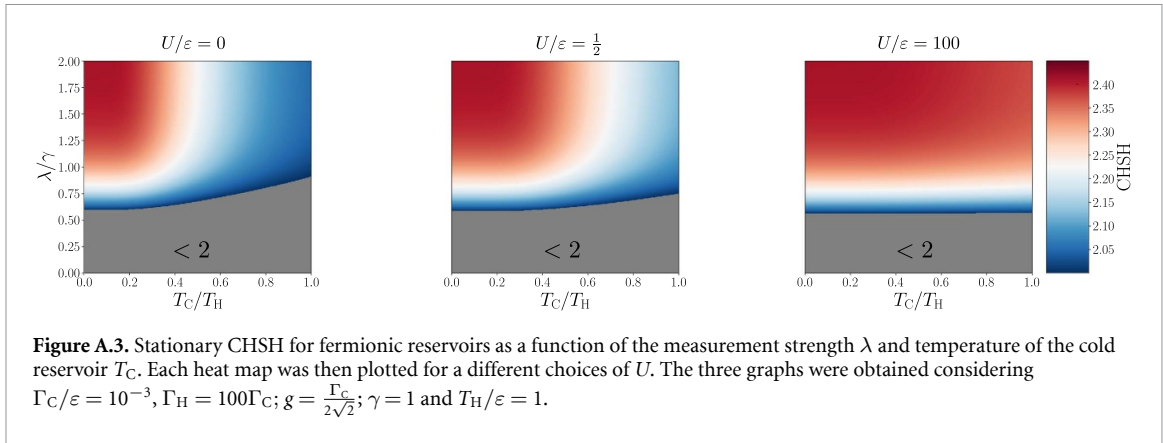


Figure A.3. Stationary CHSH for fermionic reservoirs as a function of the measurement strength λ and temperature of the cold reservoir T_C . Each heat map was then plotted for a different choices of U . The three graphs were obtained considering $\Gamma_C/\varepsilon = 10^{-3}$, $\Gamma_H = 100\Gamma_C$; $g = \frac{\Gamma_C}{2\sqrt{2}}$; $\gamma = 1$ and $T_H/\varepsilon = 1$.

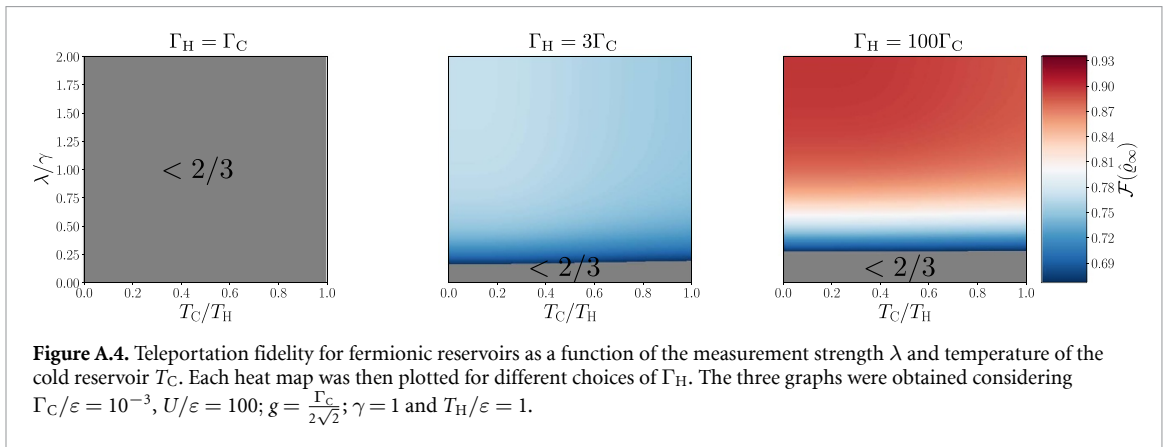


Figure A.4. Teleportation fidelity for fermionic reservoirs as a function of the measurement strength λ and temperature of the cold reservoir T_C . Each heat map was then plotted for different choices of Γ_H . The three graphs were obtained considering $\Gamma_C/\varepsilon = 10^{-3}$, $U/\varepsilon = 100$; $g = \frac{\Gamma_C}{2\sqrt{2}}$; $\gamma = 1$ and $T_H/\varepsilon = 1$.

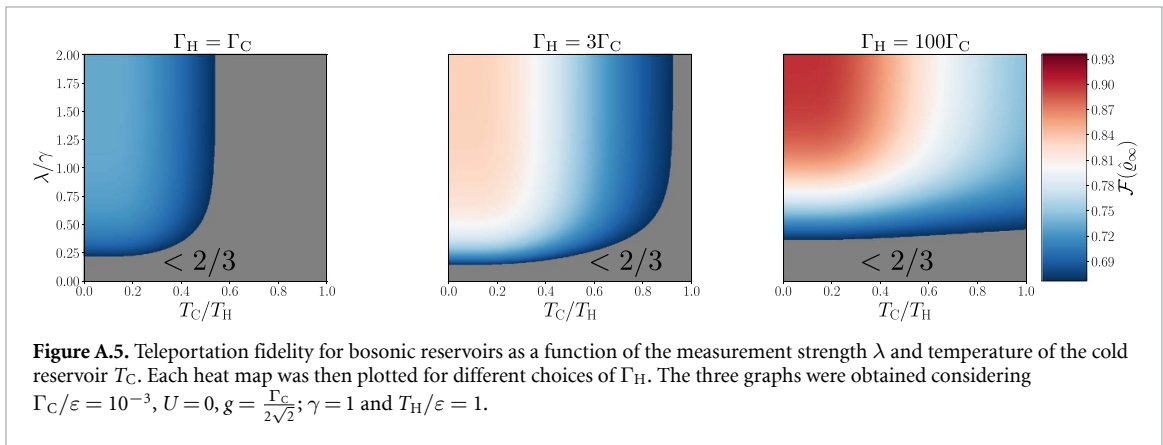


Figure A.5. Teleportation fidelity for bosonic reservoirs as a function of the measurement strength λ and temperature of the cold reservoir T_C . Each heat map was then plotted for different choices of Γ_H . The three graphs were obtained considering $\Gamma_C/\varepsilon = 10^{-3}$, $U = 0$, $g = \frac{\Gamma_C}{2\sqrt{2}}$; $\gamma = 1$ and $T_H/\varepsilon = 1$.

the region of optimal CHSH value to extend to higher values of T_C , provided a high enough measurement strength λ (note $\Gamma_H \gg \Gamma_C$).

Figure A.4 shows the teleportation fidelity of the fermionic engine as a function of λ and T_C for different choices of Γ_H . When comparing these plots with the ones for CHSH in figure A.1, we find that, in this scenario, teleportation fidelity represents a weaker condition for the usefulness of the entanglement contained in the engine, as the entanglement can uphold teleportation already for $\Gamma_H = 3\Gamma_C$, whilst, according to CHSH, we required $\Gamma_H \gg \Gamma_C$. Furthermore, we see that this is yet more apparent in the case of the bosonic engine (see figure A.5), where the entanglement produced by the engine is operationally useful already at $\Gamma_H = \Gamma_C$.

In figure A.6 we show the steady state teleportation fidelity for the fermionic engine as a function of λ and T_C , for different choices of U . As in the case of CHSH (see figure A.3) we see that increasing U allows the engine to reproduce the optimal fidelity results (see section 4) at higher temperatures for the cold bath, granted a high enough measurement strength λ .

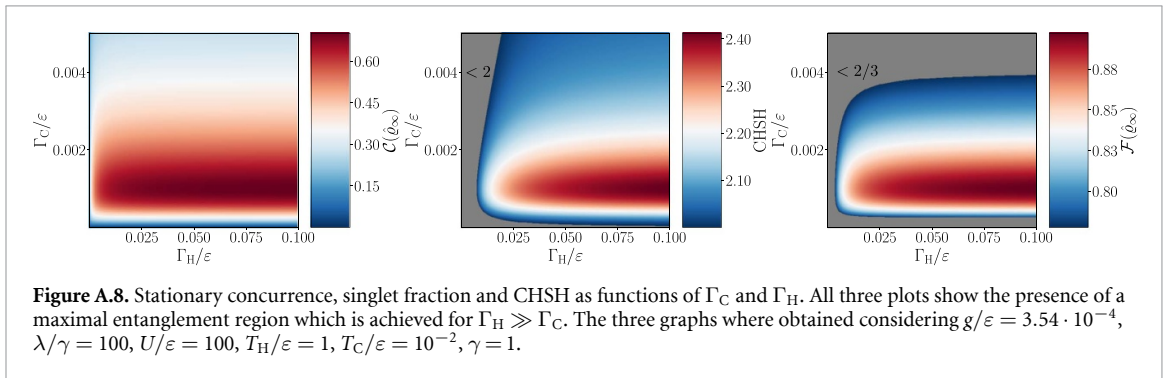
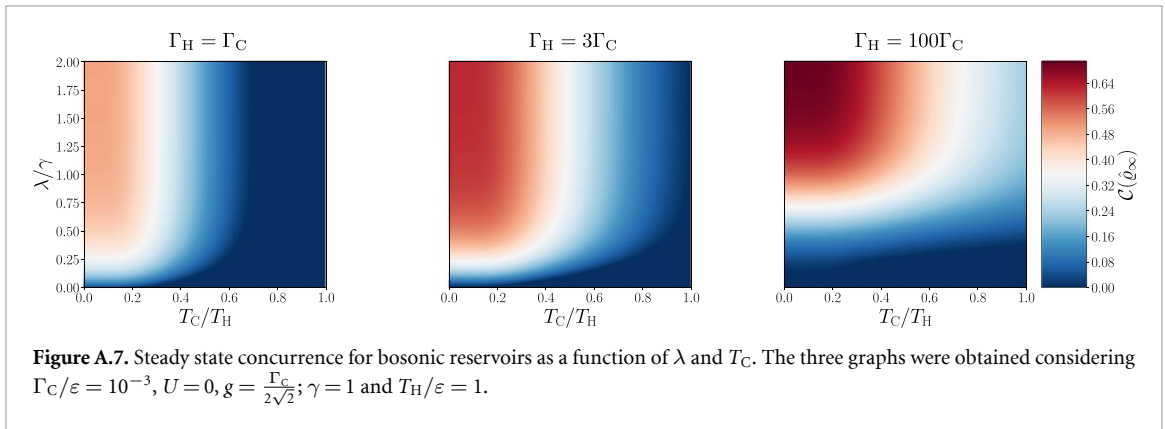
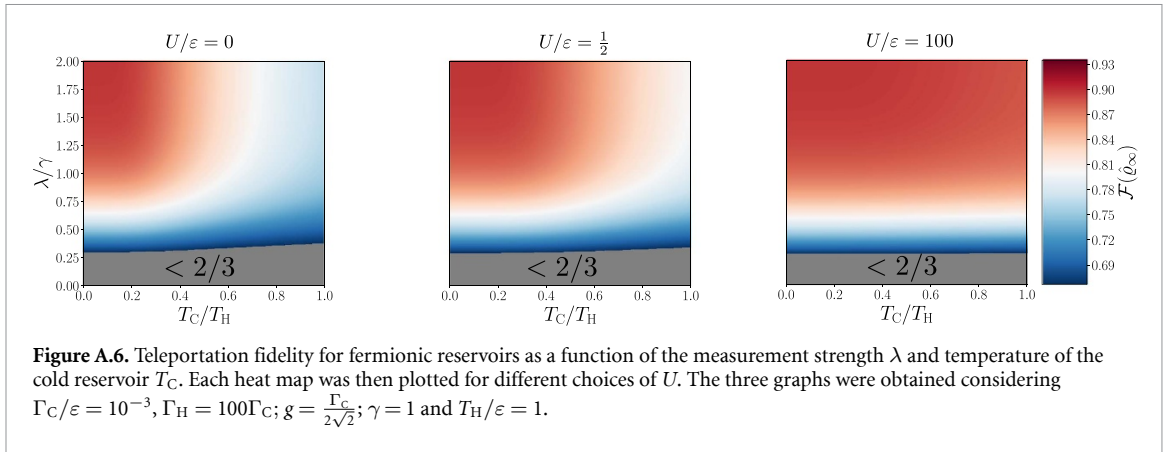


Figure A.7, shows the stationary concurrence for bosonic reservoirs as a function of λ and T_C . The results are similar to those in figure 4, where we studied fermionic reservoirs.

Lastly, figure A.8 shows the the concurrence, singlet fraction and CHSH for the steady state of the fermionic engine as a function of Γ_C and Γ_H (note that the results for the bosonic system are equivalent). From it, we note that entanglement to be produced by this system both reservoirs must be coupled (i.e. $\Gamma_H, \Gamma_C \neq 0$). Furthermore, arbitrarily increasing the value of Γ_C will result in diminishing returns, as this will introduce additional dephasing into the system (see equation (A.11)). We thus find that maximal entanglement production is achieved in the limit $\Gamma_H \gg \Gamma_C$.

ORCID iDs

Giovanni Francesco Diotallevi <https://orcid.org/0000-0001-6765-7806>

Björn Annby-Andersson <https://orcid.org/0000-0002-5570-9856>

Peter Samuelsson <https://orcid.org/0000-0001-5025-4832>

Armin Tavakoli <https://orcid.org/0000-0001-9136-7411>

Pharnam Bakhshinezhad <https://orcid.org/0000-0002-0088-0672>

References

- [1] Kosloff R and Levy A 2014 *Annu. Rev. Phys. Chem.* **65** 365–93
- [2] Mitchison M T 2019 *Contemp. Phys.* **60** 164–87
- [3] Binder F, Correa L A, Gogolin C, Anders J and Adesso G (eds) 2019 *Thermodynamics in the Quantum Regime* (Springer)
- [4] Bohr Brask J, Haack G, Brunner N and Huber M 2015 *New J. Phys.* **17** 113029
- [5] Khandelwal S, Palazzo N, Brunner N and Haack G 2020 *New J. Phys.* **22** 073039
- [6] Bohr Brask J, Clivaz F, Haack G and Tavakoli A 2022 *Quantum* **6** 672
- [7] Tavakoli A, Haack G, Huber M, Brunner N and Bohr Brask J 2018 *Quantum* **2** 73
- [8] Tavakoli A, Haack G, Brunner N and Brask J B 2020 *Phys. Rev. A* **101** 012315
- [9] Man Z X, Tavakoli A, Bohr Brask J and Xia Y J 2019 *Phys. Scr.* **94** 075101
- [10] Prech K, Johansson P, Nyholm E, Landi G T, Verdozzi C, Samuelsson P and Potts P P 2023 *Phys. Rev. Res.* **5** 023155
- [11] Wang J, Wiseman H M and Milburn G J 2005 *Phys. Rev. A* **71** 042309
- [12] Mancini S and Wang J 2005 *Eur. Phys. J. D* **32** 257–60
- [13] Carvalho A R R and Hope J J 2007 *Phys. Rev. A* **76** 010301
- [14] Carvalho A R R, Reid A J S and Hope J J 2008 *Phys. Rev. A* **78** 012334
- [15] Li J G, Zou J, Shao B and Cai J F 2008 *Phys. Rev. A* **77** 012339
- [16] Hou S C, Huang X L and Yi X X 2010 *Phys. Rev. A* **82** 012336
- [17] Annby-Andersson B, Bakhshinezhad F, Bhattacharyya D, De Sousa G, Jarzynski C, Samuelsson P and Potts P P 2022 *Phys. Rev. Lett.* **129** 050401
- [18] Barker D, Lehmann S, Namazi L, Nilsson M, Thelander C, Dick K A and Maisi V F 2019 *Appl. Phys. Lett.* **114** 183502
- [19] Barker D, Scandi M, Lehmann S, Thelander C, Dick K A, Perarnau-Llobet M and Maisi V F 2022 *Phys. Rev. Lett.* **128** 040602
- [20] Eriksson A M et al 2023 Universal control of a bosonic mode via drive-activated native cubic interactions (arXiv:2308.15320)
- [21] Wootters W K 1998 *Phys. Rev. Lett.* **80** 2245–8
- [22] Åström K J and Murray R M 2008 *Feedback Systems - An Introduction for Scientists and Engineers* (Princeton University Press)
- [23] Caves C M, Thorne K S, Drever R W, Sandberg V D and Zimmermann M 1980 *Rev. Mod. Phys.* **52** 341–92
- [24] Meyer zu Rheda C, Haack G and Romito A 2014 *Phys. Rev. B* **90** 155438
- [25] Horodecki M, Horodecki P and Horodecki R 1999 *Phys. Rev. A* **60** 1888–98